Journal of Biomedical Research

CRISPR/Cas9-mediated genome editing reveals six testis-enriched genes dispensable for male fertility in mice

Heling Fu, Haoran Chen, Chenmeijie Li, Shuai Lu, Yayun Gu, Zhibin Hu

Cite this article as:
Heling Fu, Haoran Chen, Chenmeijie Li, Shuai Lu, Yayun Gu, Zhibin Hu. CRISPR/Cas9–mediated genome editing reveals six testis–enriched genes dispensable for male fertility in mice[J]. *Journal of Biomedical Research*, 2026, 40(4): 1–14. doi: 10.7555/JBR.39.20250247

View online: https://doi.org/10.7555/JBR.39.20250247

Available online at www.jbr-pub.org.cn

Open Access at PubMed Central

Journal of Biomedical Research, 2026 40(4): 1–14

JBR

Original Article

CRISPR/Cas9-mediated genome editing reveals six testis-enriched genes dispensable for male fertility in mice

Heling Fu[1,△], Haoran Chen[1,2,△], Chenmeijie Li[1], Shuai Lu[1], Yayun Gu[1], Zhibin Hu[1,2,✉]

[1]*State Key Laboratory of Reproductive Medicine and Offspring Health, Nanjing Medical University, Nanjing, Jiangsu 211166, China;*
[2]*Department of Epidemiology, Center for Global Health, School of Public Health, Nanjing Medical University, Nanjing, Jiangsu 211166, China.*

Abstract

The genetic landscape of male infertility is highly complex. It is estimated that at least 1 000–2 000 genes are involved in human and mouse infertility. Although functional analyses have been performed on hundreds of genes, many others still have unknown functions. Generating gene-editing mice is a powerful tool for exploring whether a given gene is essential for male reproduction *in vivo*. In the current study, we investigated the function of six genes, *Efcab7*, *Tekt3*, *Mlf1*, *Rp1l1*, *Agbl2*, and *Tmsb15a*, using the CRISPR/Cas9 system. Mating tests with mutant mice revealed that all six genes are dispensable for male fecundity when individually ablated. Meanwhile, phenotypic analyses of testicular appearance and weight, testis and epididymis morphology, and sperm motility parameters in these six mutant mice also showed no significant differences compared with wild-type mice. In summary, our results suggest that these six genes could be deprioritized by other researchers interested in their roles in male infertility, thereby preventing duplicative research efforts.

Keywords: spermatogenesis, genetics of male infertility, dispensable genes, CRISPR/Cas9

Introduction

Male infertility is a global health concern, affecting more than 50 million couples worldwide according to the World Health Organization (WHO)[1]. Genetic disorders are a major reason for male infertility[2]. Next-generation sequencing technologies have identified key genes crucial for spermatogenesis, including *SPEM2*[3], autophagy-related *ATG5/ATG7*[4], and *FBXO47*[5]. Previously, our studies have also identified several genes, such as *WDR63*[6] and *CCER1*[7]. However, with more than 1 000–2 000 genes predominantly expressed in the testis[8], the pathogenic genes currently identified are only the tip of the iceberg.

Humans and mice share a high degree of genetic similarity, with approximately 99% of mouse genes having a human counterpart[9]. This genetic homology provides a strong foundation for using mice as models to study human diseases. Many genes have already been shown to decrease fertility in mouse models, indicating their indispensability for male reproduction. Meanwhile, hundreds of genes have also been identified as non-essential for male fertility, likely due

△These authors contributed equally to this work

✉Corresponding author: Zhibin Hu, E-mail: zhibin_hu@njmu.edu.cn, ORCID:0000-0002-8277-5234.

Received: 19 June 2025; Revised: 25 October 2025; Accepted: 26 October 2025; Available online: 28 October 2025

CLC number: R394.3; R698, Document code: A

The authors reported no conflict of interests. Zhibin Hu is the Editor-in-Chief of this journal and was excluded from all editorial decisions. The manuscript was handled independently, with peer review conducted by at least two external reviewers.

https://doi.org/10.7555/JBR.39.20250247

to functional redundancy. For example, studies have reported more than 20 genes, such as *Allc*[10], *Fscb*[10], *Tmem210*[11], and *4921539E11Rik*[11], that are dispensable for male fertility. Notably, patients with male infertility often seek assistance from *in vitro* fertilization or intracytoplasmic sperm injection to have their own offspring. However, there is a significant risk that pathogenic genes or variants may be transmitted to their progeny during these processes if preimplantation genetic diagnosis is not performed[12–14]. Therefore, screening the functions of as many testis-enriched genes as possible in organismal models is crucial. This approach helps identify not only genes that are dispensable for male fertility but also those critical for sperm formation and/or function. To a certain extent, it enables the protection of the genetic health of the next generation conceived through assisted reproductive technologies.

In the current study, we generated six mouse lines (*i.e.*, *Efcab7*, *Tekt3*, *Mlf1*, *Rp1l1*, *Agbl2*, and *Tmsb15a*) deficient in testis-enriched genes using the CRISPR/Cas9 system. Among these genes, five (*Efcab7*, *Tekt3*, *Mlf1*, *Rp1l1*, and *Agbl2*) were identified as carrying variants in whole-exome sequencing data from tetralogy of Fallot (TOF) cases and have been reported to be associated with cilia-related functions[15–20]; *Tmsb15a* was a cancer-testis gene[21] and speculated to play a role in sperm flagella formation. Considering the structural similarities between cilia and sperm flagella, we conducted comprehensive reproductive phenotypic analyses of these models and found that all six genes were dispensable for male fertility in mice. These findings could help avoid unnecessary and duplicated research efforts by other investigators.

Materials and methods

Animals

All animal experiments performed in the current study were approved by the Institution of Animal Care and Use Committee of Nanjing Medical University (Nanjing, China) in compliance with guidelines and regulations for animal experiments (approval: IACUC 1912049). All six mouse lines were generated using CRISPR/Cas9 techniques.

Generation of knockout (KO) mice using the CRISPR/Cas9 system

All six mouse lines in the current study were produced using the CRISPR/Cas9 genome editing system. The Cas9 plasmid (Addgene, Watertown, MA, USA) was linearized and transcribed into mRNA *in vitro* using a T7 Transcription Kit (Ambion, Austin, TX, USA). The single guide RNAs (sgRNAs) used in the current study are listed in ***Supplementary Table 1***. Cas9 mRNA and sgRNA were microinjected into the fertilized super-ovulated wild-type C57BL/6 female mouse zygotes, which had been mated with wild-type C57BL/6 male mice. After injection, the zygotes were transferred into the oviducts of pseudo-pregnant ICR females. Homozygous and heterozygous KO mice were obtained through sibling crosses of F1 offspring.

Genome DNA was collected from tail biopsies, and the mutation of the target gene was confirmed by PCR and Sanger sequencing. The primers and PCR conditions for genotyping are listed in ***Supplementary Table 2***.

RNA extraction, reverse transcription PCR (RT-PCR) and quantitative real-time RT-PCR (qRT-PCR)

Total RNA was extracted and purified from multiple adult tissues using the TRIzol reagent (Vazyme, Nanjing, China) according to the manufacturer's instructions, and was reverse transcribed into cDNA using the HiScript Ⅱ Q RT SuperMix (Vazyme). All tissues, including the heart, liver, spleen, lung, kidney, brain, muscle, testis, colon, and stomach, were collected from adult C57BL/6J mice. RT-PCR was performed using 2× Phanta Max Master Mix (Dye Plus) (Vazyme), and the products were separated by electrophoresis on an agarose gel. qRT-PCR was carried out using ChamQ Universal SYBR qPCR Master Mix (Vazyme) on a QuantStudio™ 7 Flex Real-Time PCR System (Thermo Fisher Scientific, Waltham, MA, USA). Relative mRNA levels were normalized to the endogenous *Gapdh* gene (internal control). Primers used for PCR are listed in ***Supplementary Table 3***.

Phylogenetic tree analysis

Phylogenetic trees (method: UPGMA) for each gene were constructed using DNAMAN software (version 7.212, Lynnon Corp., Quebec, Canada) based on alignments of the amino acid sequences from *Homo sapiens, Mus musculus,* and other mammal species. The sequences were downloaded from the NCBI database.

Fertility test

Sexually mature C57BL/6 wild-type or KO/knock-in (KI) male mice were housed individually with two adult wild-type (WT) female mice for at least two months. Male mice were removed after a vaginal plug

was detected, and females were kept for another three weeks to count the final litters. The number of vaginal plugs and pups was checked and counted every morning.

Morphological and histological analysis of the testis and epididymis

The testes and epididymides were extracted from at least three WT and KO male mice following euthanasia. After photographing and measuring the body and testicular weights, the testes and epididymides were fixed in modified Davidson's fluid for 48 h. Subsequently, the organs and tissues were dehydrated, embedded in paraffin, and cut into 5-μm-thick slices. After deparaffinization with xylene, the sections of the testes and epididymides were stained with periodic acid-Schiff (PAS) and Mayer's hematoxylin and eosin (HE), respectively. The sections were then imaged and observed using an Olympus BX microscope equipped with an Olympus DP20 color camera (Olympus, Tokyo, Japan).

Computer-assisted sperm analysis (CASA)

Sperm from each mutant mouse and age-matched WT C57BL/6 controls were collected from the cauda epididymis, suspended in human tubal fluid (HTF) culture medium (InVitroCare, Frederick, MD, USA), and maintained at 37 ℃. The sperm were then diluted, placed on an 80 μm chamber slide, and analyzed using the Ceros Ⅱ analyzer (Hamilton Thorne, Beverly, MA, USA). The proportion of motile spermatozoa, the percentage of progressively motile spermatozoa, and the spermatozoa concentration (M/mL) were measured and analyzed.

Morphological analysis of spermatozoa

Three male mice from each KO/KI line and age-matched WT C57BL/6 controls were used for malformation analysis. Cauda epididymal spermatozoa were suspended in human sperm suspension fluid culture medium (InVitroCare), and 10 μL of epididymal sperm suspension fluid was placed and spread out on a poly-L-lysine (PLL)-coated glass slide. The slides were air-dried and then immersed in 4% paraformaldehyde fluid for 1 h. The slides were stained with HE solution prior to imaging and observed using an Olympus BX microscope equipped with an Olympus DP20 color camera (Olympus). At least 200 sperm on each slide were counted, and abnormal sperm were labeled using ImageJ software.

Protein extraction and Western blot analysis

Mouse testicular tissues were collected after removal of the tunica albuginea. The samples were lysed in RIPA buffer (Beyotime, Shanghai, China) supplemented with a protease inhibitor cocktail (MedChemExpress, Monmouth Junction, NJ, USA), followed by ultrasonication and incubation on ice for 30 min. After centrifugation at 4 ℃, the supernatant was collected and mixed with 2× SDS loading buffer (Applygen, Beijing, China). Proteins were denatured by heating at 100 ℃ for 10 min. The denatured proteins were then separated on an SDS-polyacrylamide gel and transferred to a polyvinylidene fluoride (PVDF) membrane (Millipore, Billerica, MA, USA) for immunoblot analysis. The antibodies used in the current study were: mouse anti-MLF1 (1 ∶ 250, Cat. #sc-514 294, Santa Cruz Biotechnology, Santa Cruz, CA, USA), rabbit anti-GAPDH (1 ∶ 1 000, Cat. #2118L, Cell Signaling Technology, Danvers, MA, USA), anti-mouse IgG HRP (1 ∶ 2 000, Cat. #A0216, Beyotime), and anti-rabbit IgG HRP (1 ∶ 2 000, Cat. #A0208, Beyotime).

Statistical analysis

Statistical analysis was performed using a two-tailed unpaired Student's *t*-test with statistical significance set at a P value of < 0.05. All data are represented as the mean ± standard deviation (SD) from at least three replicates for each experiment. Microsoft Excel and GraphPad Prism 9 were used for statistical analysis.

Results

Expression patterns and conservation analyses of candidate genes

Cilia and sperm flagella both share the "9 + 2" structure (***Fig. 1A***), and any alteration in their structure or function can lead to serious diseases, such as primary ciliary dyskinesia[22–23] and male infertility[6]. Here, we explored the function of six genes with different subcellular localizations in cilia (***Fig. 1A***). Among these genes, *EFCAB7* is situated within the ciliary membrane[15], while *MLF1*[18] and *TMSB15A*[15] are found in the cytoplasm; *AGBL2*[20] is localized to the centriole and, along with *MLF1*[18] and *EFCAB7*[16], is also localized to the basal body. Additionally, *TEKT3*[17] and *RP1L1*[19] are associated with axonemal microtubules. To further investigate the function of these six genes in male fertility using mouse models, we first ensured that the target genes met two criteria: (i) testis-enriched expression to minimize potential side effects in other systems and (ii) the presence of a mouse ortholog for functional

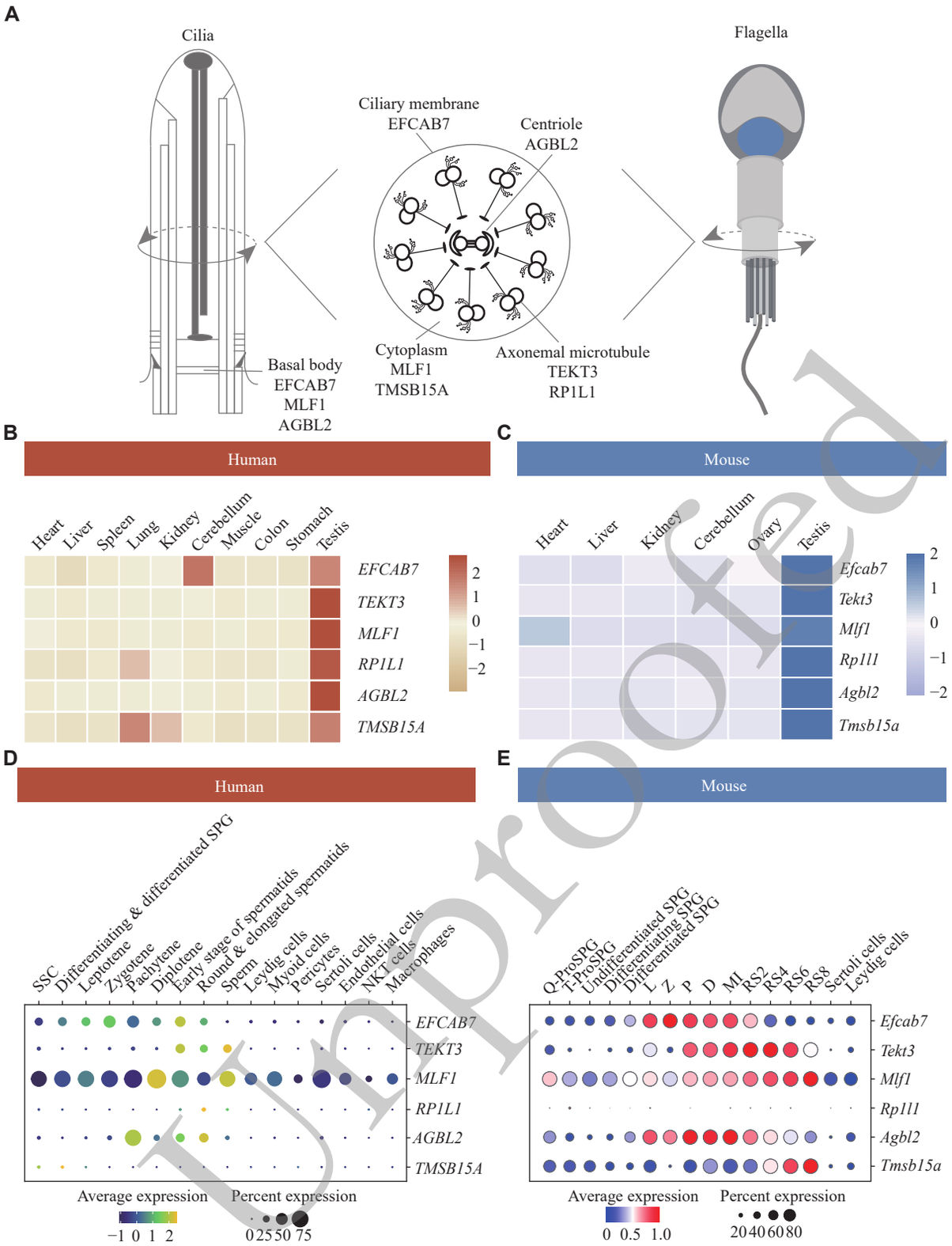

Fig. 1 **Subcellular localization and expression patterns of specific genes in humans and mice.** A: Schematic diagram of cilia and sperm flagella with the subcellular localization of six genes depicted. B: Expression of the six genes in different human tissues. Data sourced from the GTEx public database. C: Expression of the six genes in different mouse tissues. Data sourced from a published literature[44]. D: Single-cell expression of the six genes during human spermatogenesis. E: Single-cell expression of the six genes during mouse spermatogenesis. Abbreviations: L, leptotene; D, diplotene; M I (meiotic I); P, pachytene; Q-ProSPG, quiescent progenitor spermatogonia; RS2–RS8, round spermatids at steps 2–8; SPG, spermatogonia; SSC, spermatogonial stem cell; T-ProSPG, transit-amplifying progenitor spermatogonia; Z, zygotene.

validation. As shown in ***Fig. 1B*** and ***1C***, all six genes were predominantly expressed in the testes of both humans and mice. To confirm this, we extracted RNA from multiple mouse tissues, including the heart, liver, spleen, testis, *etc.*, and performed conventional RT-PCR and qRT-PCR. The results consistently showed a testis-enriched expression pattern for all six genes (***Supplementary Fig. 1A***). *Rp1l1* also exhibited considerable expression in other murine tissues, such as the lung, in addition to its enrichment in the testis. Using single-cell RNA sequencing (scRNA-seq) data generated from human and mouse spermatogenic cells at different stages, we found that these six genes exhibited varying expression levels throughout the spermatogenesis process (***Fig. 1D*** and ***1E***). *Efcab7* and *Agbl2* showed elevated expression at the early stage of spermatids or pachytene in both humans and mice; *Tekt3*, *Mlf1*, and *Tmsb15a* showed varying expression biases during different stages of spermatogenesis in humans and mice, suggesting a degree of heterogeneity between species. Although *Rp1l1* is enriched in the testis, scRNA-seq data showed very low expression levels in all cells during spermatogenesis, including those in the microenvironment.

Moreover, to understand the evolutionary conservation of these candidate genes among mammals, we constructed phylogenetic trees and found that all genes were conserved in humans (***Supplementary Fig. 1B***).

Generation of mutant mouse lines

To investigate the essentiality of six candidate target genes in spermatogenesis, we generated six mutant mouse lines using the CRISPR/Cas9 technology. The mutant alleles were detected by genomic PCR and confirmed by Sanger sequencing. The mutated loci of all mutant mouse lines are summarized in ***Supplementary Table 1***. The primers used for genotyping and their annealing temperatures are shown in ***Supplementary Table 2***.

Fertility tests of mutant male mice

To examine the fecundity of these mutant males, individual mutant male mice were caged with up to two wild-type female mice for at least two months. The fecundity of three wild-type males was tested in parallel as positive controls. The average litter size of each mutant male showed that they could produce litters comparable to those of the WT controls, at approximately eight pups per litter (***Table 1***). Thus, all mutant males in this study exhibited normal fertility.

Phenotypic analyses of mutant males

Although all mutant males had normal fertility, we conducted detailed analyses of reproductive phenotypes, including testicular and sperm development, for each mutant line.

Our team previously reported that *Efcab7* mutant mice exhibited hindered ciliary transport and disrupted cardiac development[24]. Briefly, we generated *Efcab7* mutant lines by designing an sgRNA targeting the upstream of exon 6 in intron 5 of the *Efcab7* gene, resulting in a G>C substitution at the splicing site. These changes were confirmed by genomic PCR and Sanger sequencing (***Fig. 2A*** and ***2B***), mimicking the variant detected in one TOF case (***Supplementary Table 4***). Primers used for genotyping are summarized in ***Supplementary Table 2***. In addition to cardiac phenotypes, we also detected their reproductive phenotypes. No statistically significant difference was observed in the testis size and weights between the wild-type and homozygous knock-in mice (***Fig. 2C*** and ***2D***). Similar to control samples, histological sections of knock-in testes and epididymides showed normal spermatogenesis in the seminiferous tubules and normal sperm morphology and density in the cauda epididymides (***Fig. 2E***). Moreover, CASA

Table 1 **Male fertility of six mouse lines**

Gene symbol	Genotype	No. of males	No. of pups	No. of litters	Mating period (weeks)	Average litter size (mean ± SD)
Wildtype	+/+	4	105	12	8	8.7 ± 1.4
Efcab7	c.509-1G>C/c.509-1G>C	3	98	12	8	8.2 ± 1.6
Tekt3	−76bp/−76bp	3	66	8	8	8.3 ± 0.9
Mlf1	R243*/R243*	4	150	16	12	9.4 ± 1.3
Rp1l1	−7bp/−7bp	3	114	14	8	8.1 ± 1.3
Agbl2	−11bp/−11bp	3	96	12	8	8.0 ± 0.9
Tmsb15a	−191bp, G>A/Y	3	98	12	8	8.2 ± 1.2

Abbreviation: SD, standard deviation.

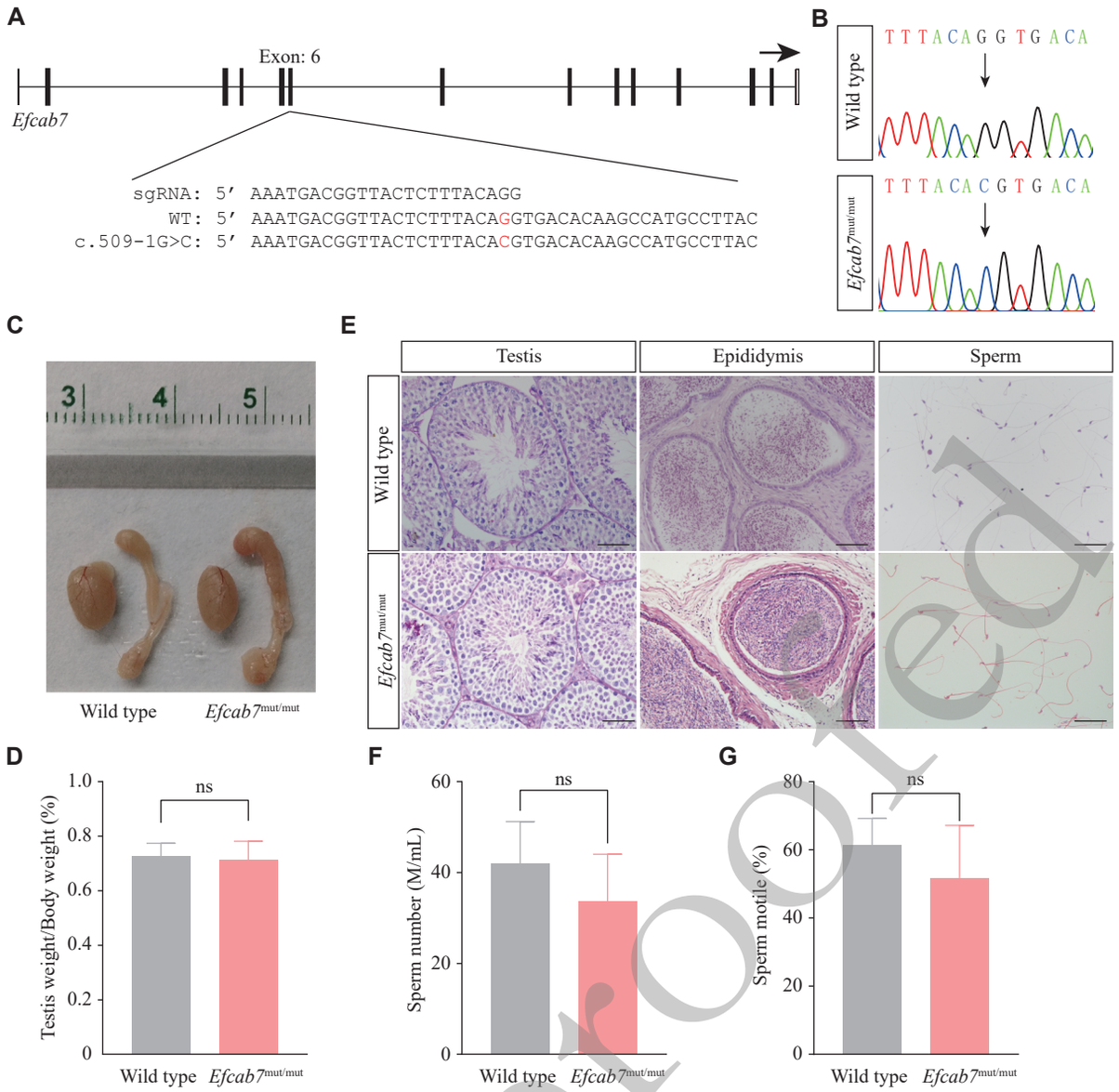

Fig. 2 **Phenotypic analysis of *Efcab7*$^{mut/mut}$ male mice.** A: Gene editing strategy for *Efcab7*. An sgRNA was designed to target upstream of exon 6 in intron 5. B: Genotyping of *Efcab7*$^{mut/mut}$ mice through PCR and subsequent Sanger sequencing. Arrows indicate the mutant alleles. C: Morphology of the testes from wild-type and *Efcab7*$^{mut/mut}$ mice. A cm-scale ruler is shown above for size reference. D: Comparison of testis weight to body weight between wild-type mice and *Efcab7*$^{mut/mut}$ mice. n = 3 males per group. E: Histological analysis of the testes, epididymides, and sperm in wild-type and *Efcab7*$^{mut/mut}$ mice. All tissue sections and sperm smears were stained with HE, except for the testis sections from *Efcab7*$^{mut/mut}$ mice, which were stained with PAS.Scale bars, 50 μm (testes), 100 μm (epididymides), and 50 μm (sperm). F: Comparison of sperm concentration between wild-type and *Efcab7*$^{mut/mut}$ mice. n = 3 males per group. M/mL, million per milliliter. G: Comparison of sperm motility between wild-type and *Efcab7*$^{mut/mut}$ mice. n = 3 males per group. Quantitative data of D, F and G are presented as mean ± standard deviation (SD), and statistical analysis was performed using two-tailed unpaired Student's t-test. ns, not significant.

results revealed that *Efcab7*$^{mut/mut}$ spermatozoa exhibited normal concentration and motility compared with control spermatozoa (***Fig. 2F*** and ***2G***).

Tekt3 is a gene containing eight exons. To disrupt this gene, we designed two sgRNAs targeting exon 2 (***Fig. 3A***), resulting in a 76-bp deletion of exon 2 (***Fig. 3B***). Primers used for identifying the mutant allele are presented in ***Supplementary Table 2***. The *Tekt3* knockout mice were viable, and no statistically significant difference was observed in the testis sizes and weights between the homozygous KO and WT mice (***Fig. 3C*** and ***3D***). Morphological and histological analyses of *Tekt3*$^{-/-}$ testes and epididymides were then performed. The results showed that histological sections of KO testes and epididymides exhibited normal morphology and structure compared with WT controls (***Fig. 3E***). CASA also revealed that *Tekt3*$^{-/-}$ spermatozoa

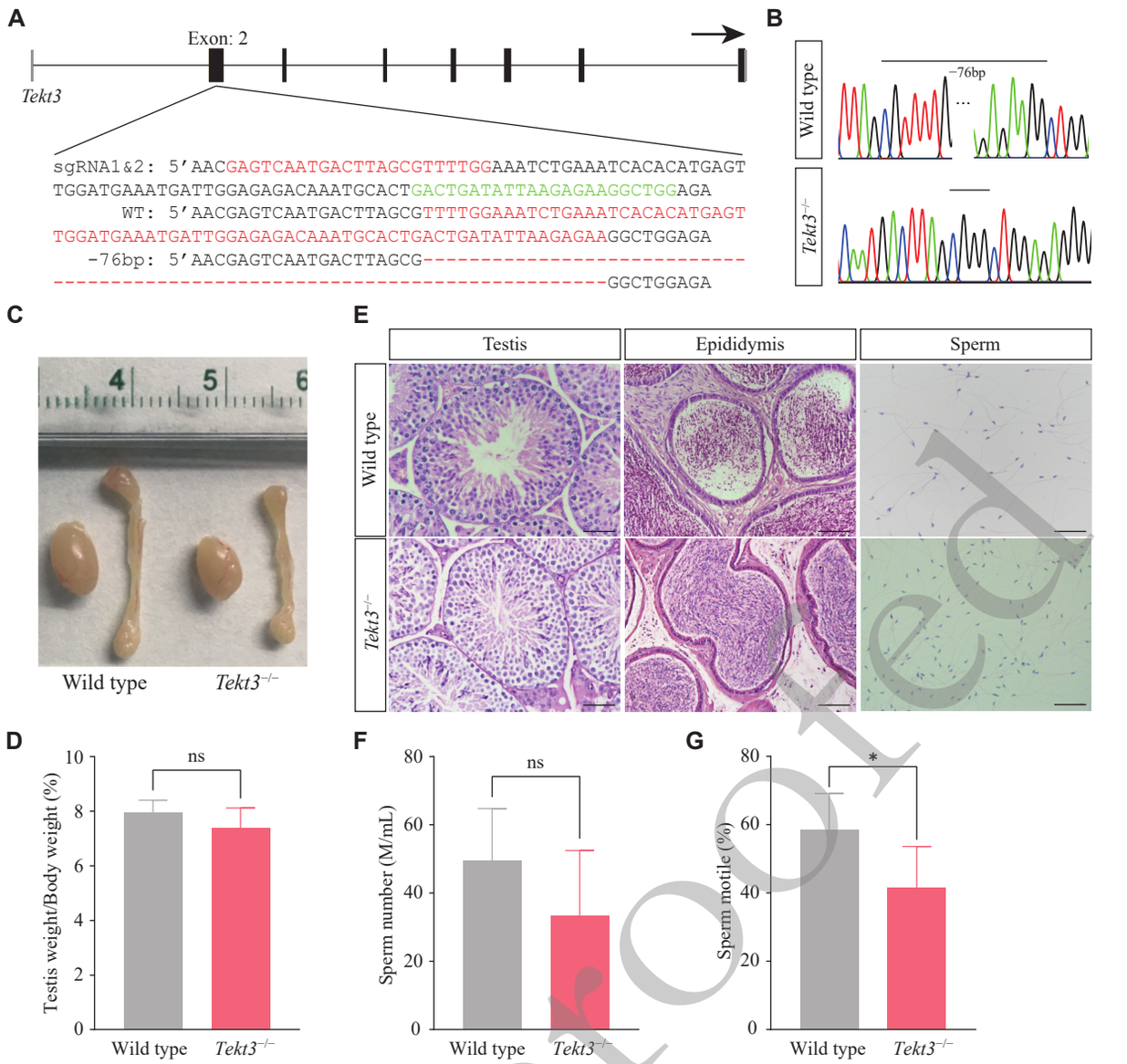

Fig. 3 **Phenotypic analysis of *Tekt3*$^{-/-}$ male mice.** A: Gene editing strategy for *Tekt3*. Two sgRNAs were designed to target exon 2 of *Tekt3*. B: Genotyping of *Tekt3*$^{-/-}$ mice through PCR and subsequent Sanger sequencing. Lines indicate the mutant alleles. C: Morphology of testes from wild-type and *Tekt3*$^{-/-}$ mice. A cm-scale ruler is shown above for size reference. D: Comparison of testis weight to body weight between wild-type mice and *Tekt3*$^{-/-}$ mice. n = 3 males per group. E: Histological analysis of the testes, epididymides, and sperm in wild-type and *Tekt3*$^{-/-}$ mice. All tissue sections and sperm smears were stained with HE, except for the testis sections from *Tekt3*$^{-/-}$ mice, which were stained with PAS Scale bars, 50 μm (testes), 100 μm (epididymides), and 50 μm (sperm). F: Comparison of sperm concentration between wild-type and *Tekt3*$^{-/-}$ mice. n = 3 males per group. M/mL, million per milliliter. G: Comparison of sperm motility between wild-type and *Tekt3*$^{-/-}$ mice. n = 3 males per group. Quantitative data of D, F and G are presented as mean ± standard deviation (SD), and statistical analysis was performed using two-tailed unpaired Student's t-test. ns, not significant.

exhibited normal concentration compared with control spermatozoa (***Fig. 3F***). We also observed that the motility of *Tekt3*$^{-/-}$ spermatozoa was relatively lower than that of WT spermatozoa; however, the motility of *Tekt3*$^{-/-}$ spermatozoa exceeded 40%, and *Tekt3*$^{-/-}$ male mice were fertile. To investigate the underlying cause of reduced sperm motility in *Tekt3*$^{-/-}$ male mice, we conducted comprehensive morphological analyses of over 300 sperm from both WT and *Tekt3*$^{-/-}$ mice separately. The results showed no significant differences in head morphology between the two groups, but *Tekt3*$^{-/-}$ males frequently exhibited prominent flagellar bending, with an incidence of 9.99% compared with 3.25% in WT mice (***Supplementary Table 5***). This structural defect in *Tekt3*$^{-/-}$ sperm impaired forward movement, contributing to decreased motility. These results suggest that a male infertility phenotype may occur when sperm motility declines to a certain level.

Mlf1 is located in the cytoplasm and the cilium

basal body. To disrupt *Mlf1*, we designed an sgRNA targeting its exon 7 to mimic the nonsense variant detected in one TOF case (***Fig. 4A***, ***Supplementary Table 4***). Then, we performed PCR using primers presented in ***Supplementary Table 2*** to identify the mutant allele. Mutant mice carrying a CGG>TGA transition (R243*) were confirmed by PCR and Sanger sequencing (***Fig. 4B***). qRT-PCR analysis demonstrated that the mutation led to a significant downregulation of *Mlf1* mRNA expression ($P < 0.01$; ***Supplementary Fig. 2A***), which was accompanied by decreased protein abundance (***Supplementary Fig. 2B***). The observed protein reduction was moderate, likely due to the mutation's distal position within the coding region. We found that the testis size, weight, and histology of *Mlf1*$^{R243*/R243*}$ males were comparable to those of control mice (***Fig. 4C–4E***). Additionally, there were no significant differences between wild-type and mutant males in sperm concentration and the percentage of motile spermatozoa (***Fig. 4F*** and ***4G***).

Rp1l1 was mutated using two sgRNAs targeting exon 4 (***Fig. 5A***). Primers for detecting the mutant

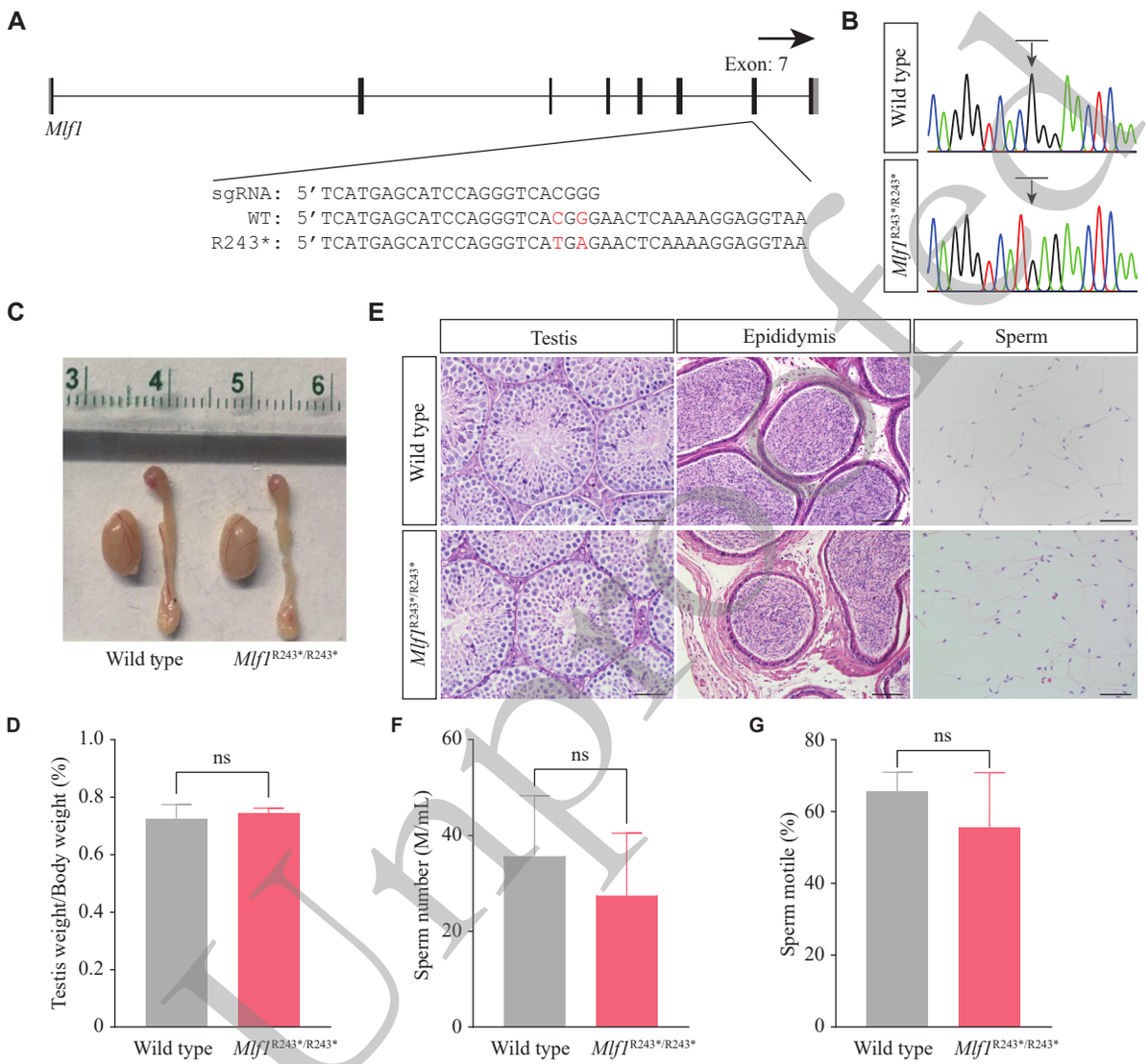

Fig. 4 **Phenotypic analysis of *Mlf1*$^{R243*/R243*}$ male mice.** A: Gene editing strategy for *Mlf1*. An sgRNA was designed to target exon 7 of *Mlf1*. B: Genotyping of *Mlf1*$^{R243*/R243*}$ mice through PCR and subsequent Sanger sequencing. Arrows indicate the mutant alleles. C: Morphology of the testes from wild-type and *Mlf1*$^{R243*/R243*}$ mice. A cm-scale ruler is shown above for size reference. D: Comparison of testis weight to body weight between wild-type mice and *Mlf1*$^{R243*/R243*}$ mice. $n = 3$ males per group. E: Histological analysis of the testes, epididymides, and sperm in wild-type and *Mlf1*$^{R243*/R243*}$ mice. All tissue sections and sperm smears were stained with HE, except for the testis sections, which were stained with PAS. Scale bars, 50 μm (testes), 100 μm (epididymides), and 50 μm (sperm). F: Comparison of sperm concentration between wild-type and *Mlf1*$^{R243*/R243*}$ mice. $n = 3$ males per group. M/mL, million per milliliter. G: Comparison of sperm motility between wild-type and *Mlf1*$^{R243*/R243*}$ mice. $n = 3$ males per group. Quantitative data of D, F and G are presented as mean ± standard deviation (SD), and statistical analysis was performed using two-tailed unpaired Student's t-test. ns, not significant.

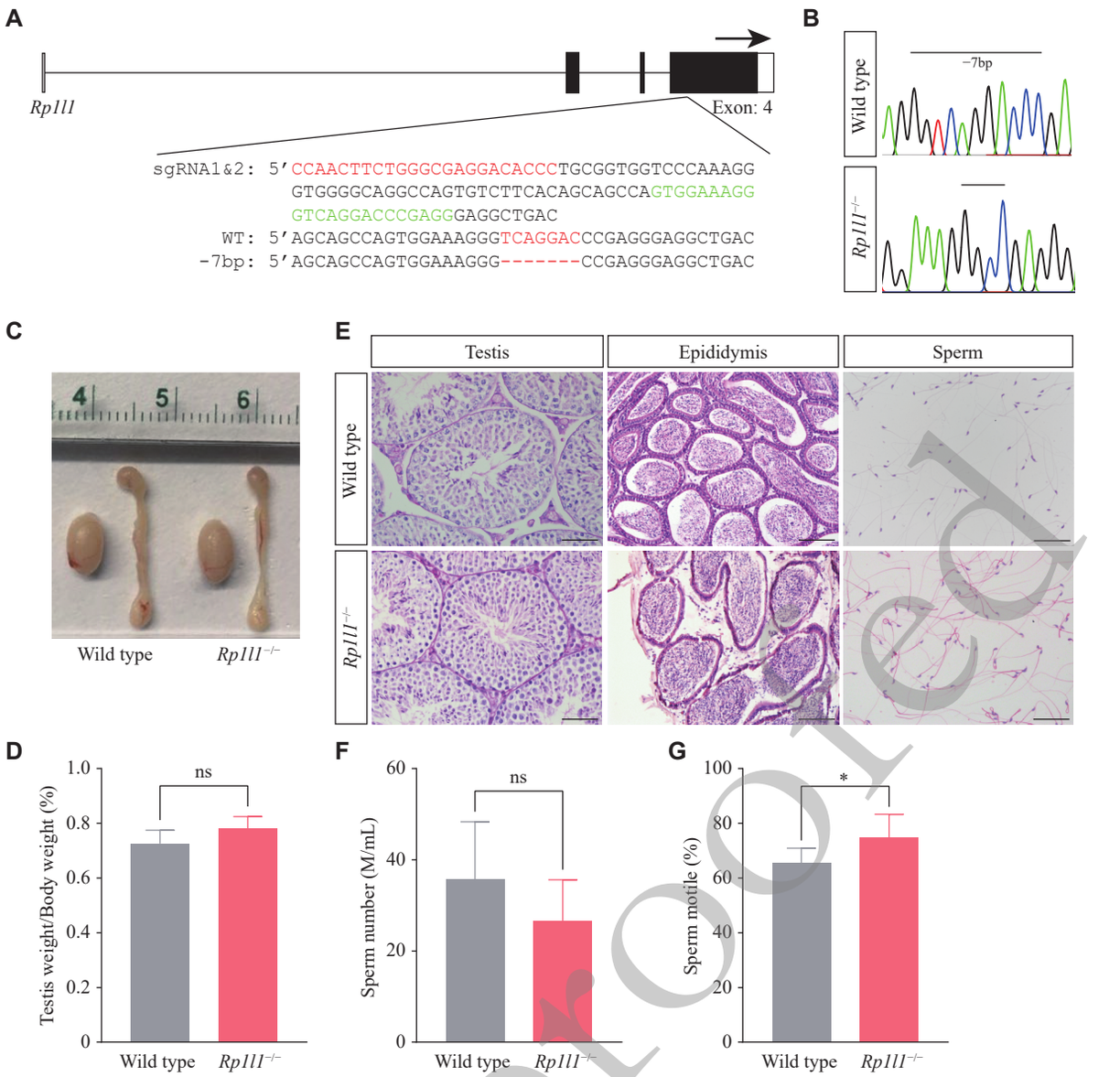

Fig. 5 **Phenotypic analysis of *Rp1l1*$^{-/-}$male mice.** A: Gene editing strategy for *Rp1l1*. Two sgRNAs were designed to target exon 4 of *Rp1l1*. B: Genotyping of *Rp1l1*$^{-/-}$ mice through PCR and subsequent Sanger sequencing. Lines indicate the mutant alleles. C: Morphology of the testis from wild-type and *Rp1l1*$^{-/-}$ mice. A cm-scale ruler is shown above for size reference. D: Comparison of testis weight to body weight between wild-type mice and *Rp1l1*$^{-/-}$ mice. n = 3 males per group. E: Histological analysis of the testes, epididymides, and sperm in wild-type and *Rp1l1*$^{-/-}$ mice. All tissue sections and sperm smears were stained with HE, except for the testis sections from *Rp1l1*$^{-/-}$ mice, which were stained with PAS. Scale bars, 50 μm (testes), 200 μm (epididymides), and 50 μm (sperm). F: Comparison of sperm concentration between wild-type and *Rp1l1*$^{-/-}$ mice. n = 3 males per group. M/mL, million per milliliter. G: Comparison of sperm motility between wild-type and *Rp1l1*$^{-/-}$ mice. n = 3 males per group.Quantitative data of D, F and G are presented as mean ± standard deviation (SD), and statistical analysis was performed using two-tailed unpaired Student's t-test. ns, not significant.

alleles are presented in ***Supplementary Table 2***. The resulting mutant allele, carrying a 7-bp deletion in exon 4, was confirmed by PCR and Sanger sequencing (***Fig. 5B***). We then collected and analyzed the morphological and histological features of the testes and epididymides. We found no significant differences in testis appearance (***Fig. 5C***), testis weight (***Fig. 5D***), and testis histology (***Fig. 5E***). The results of CASA also confirmed that homozygous adult *Rp1l1*$^{-/-}$ male mice displayed normal sperm concentration (***Fig. 5F***) and even had more motile spermatozoa compared with the wild-type mice (***Fig. 5G***).

One sgRNA was used to target exon 8 of *Agbl2*, resulting in an 11-bp deletion in exon 8 (***Fig. 6A***). Their genotypes were confirmed by PCR with the primers shown in ***Supplementary Table 2***. Sanger sequencing revealed that the mutant mouse had an 11-bp deletion (***Fig. 6B***). Homozygous *Agbl2*$^{-/-}$ mice were viable. No significant differences were found in the morphology of the testis (***Fig. 6C***) and the testis

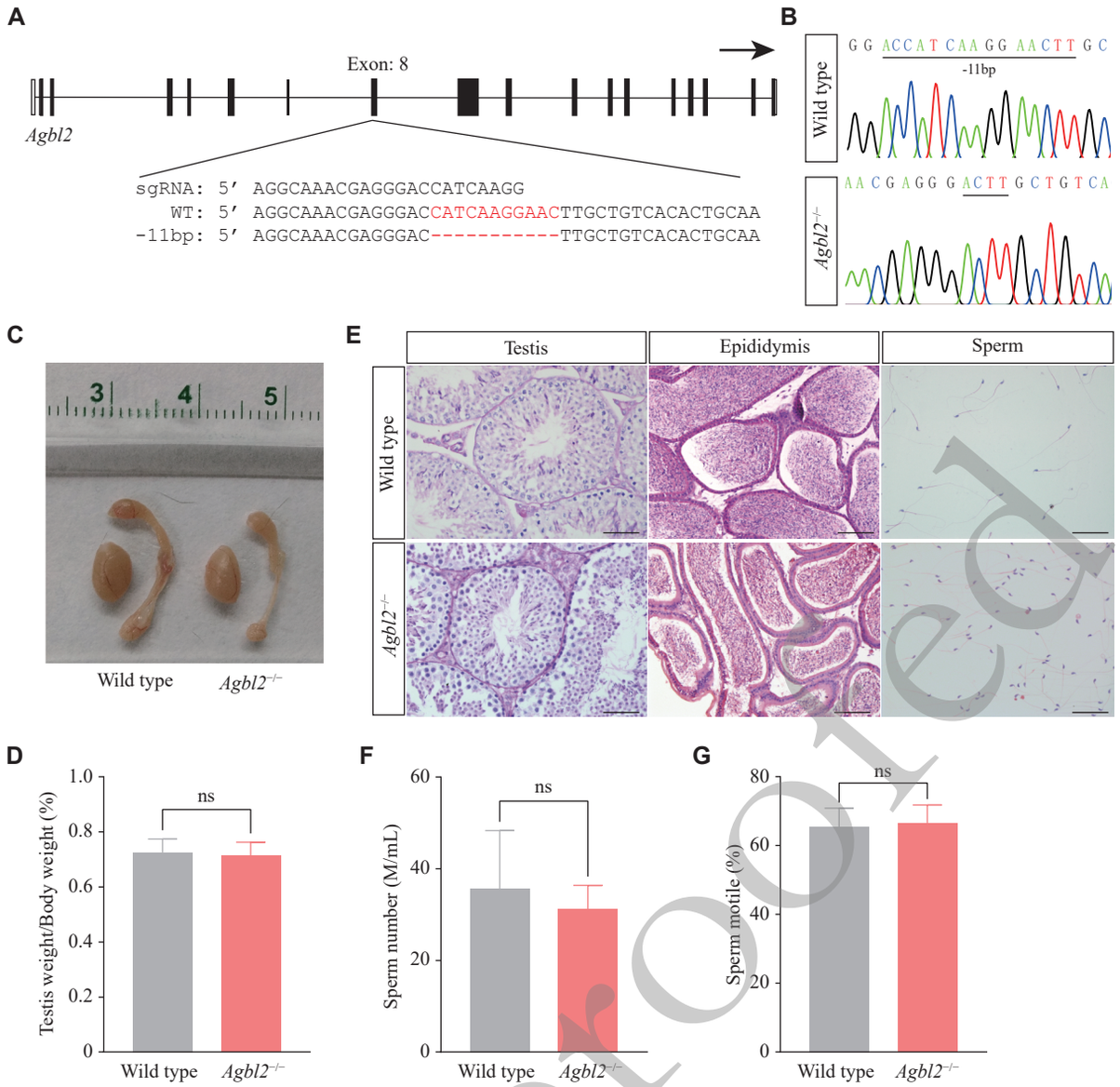

Fig. 6 **Phenotypic analysis of *Agbl2*$^{-/-}$ male mice.** A: Gene editing strategy for *Agbl2*. An sgRNA was designed to target exon 8 of *Agbl2*. B: Genotyping of *Agbl2*$^{-/-}$ mice through PCR and subsequent Sanger sequencing. Lines indicate the mutant alleles. C: Morphology of the testes from wild-type and *Agbl2*$^{-/-}$ mice. A cm-scale ruler is shown above for size reference. D: Comparison of testis weight to body weight between wild-type mice and *Agbl2*$^{-/-}$ mice. n = 3 males per group. E: Histological analysis of the testes, epididymides, and sperm in wild-type and *Agbl2*$^{-/-}$ mice. All tissue sections and sperm smears were stained with HE, except for the testis sections from *Agbl2*$^{-/-}$ mice, which were stained with PAS. Scale bar, 50 μm (testes), 100 μm (epididymides), and 50 μm (sperm). F: Comparison of sperm concentration between wild-type and *Agbl2*$^{-/-}$ mice. n = 3 males per group. M/mL, million per milliliter. G: Comparison of sperm motility between wild-type and *Agbl2*$^{-/-}$ mice. n = 3 males per group. Quantitative data of D, F and G are presented as mean ± standard deviation (SD), and statistical analysis was performed using two-tailed unpaired Student's t-test. ns, not significant.

weight/body weight ratio (***Fig. 6D***). Histological analyses of the testes and epididymides from *Agbl2*$^{-/-}$ male mice revealed no abnormalities or defects in any stage of spermatogenesis and spermatozoa morphology compared with control testis and epididymis sections (***Fig. 6E***). The CASA results of *Agbl2*$^{-/-}$ mice showed no statistical differences in sperm concentration (***Fig. 6F***) and sperm motility (***Fig. 6G***).

Tmsb15a$^{-/Y}$ mice were generated using one sgRNA designed to disrupt exon 2 (***Fig. 7A***), resulting in a 191-bp deletion and a 1-bp mutation, which led to the complete loss of exon 2. Genotyping was validated by PCR and Sanger sequencing (***Fig. 7B***). Primers used for identifying the mutant alleles are summarized in ***Supplementary Table 2***. Like all previously mentioned mutant mice, no obvious changes in the morphology of *Tmsb15a*$^{-/Y}$ testes were observed (***Fig. 7C***), and no significant differences were found in the testis weight/body weight compared with wild-

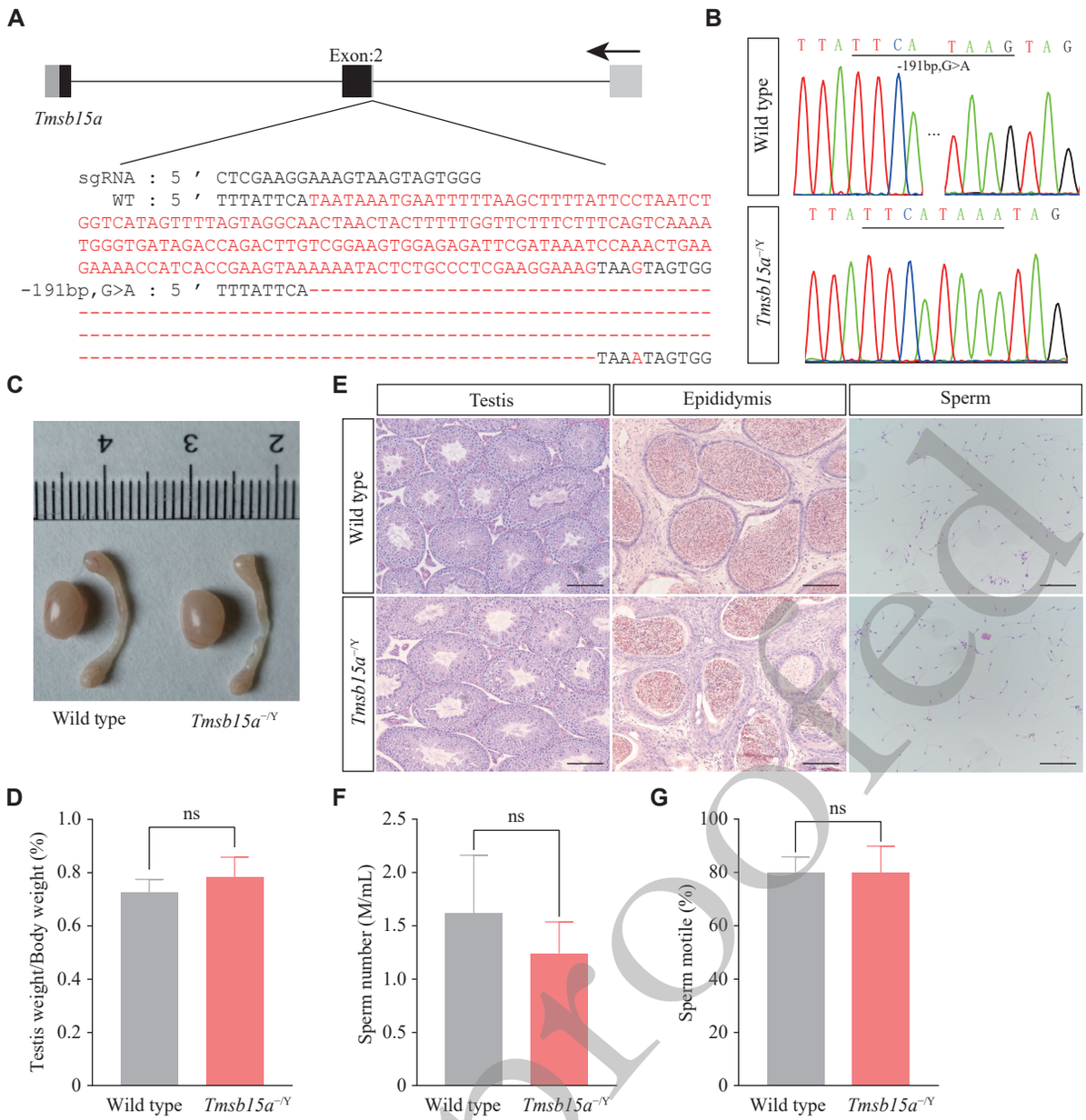

Fig. 7 **Phenotypic analysis of *Tmsb15a*$^{-/Y}$ male mice.** A: Gene editing strategy for *Tmsb15a*. An sgRNA was designed to target exon 2 of *Tmsb15a*. B: Genotyping of *Tmsb15a*$^{-/Y}$ mice through PCR and subsequent Sanger sequencing. Lines indicate the mutant alleles. C: Morphology of the testes from wild-type and *Tmsb15a*$^{-/Y}$ mice. A cm-scale ruler is shown above for size reference. D: Comparison of testis weight to body weight between wild-type mice and *Tmsb15a*$^{-/Y}$ mice. n = 3 males per group. E: Histological analysis of the testes, epididymides, and sperm in wild-type and *Tmsb15a*$^{-/Y}$ mice. All tissue sections and sperm smears were stained with HE, except for the testis sections, which were stained with PAS. Scale bars, 100 μm (testes), 100 μm (epididymides), and 100 μm (sperm). F: Comparison of sperm concentration between wild-type and *Tmsb15a*$^{-/Y}$ mice. n = 3 males per group. M/mL, million per milliliter. G: Comparison of sperm motility between wild-type and *Tmsb15a*$^{-/Y}$ mice. n = 3 males per group. Quantitative data of D, F and G are presented as mean ± standard deviation (SD), and statistical analysis was performed using two-tailed unpaired Student's t-test. ns, not significant.

type mice (***Fig. 7D***). Histological analyses of *Tmsb15a*$^{-/Y}$ testes and epididymides showed that all stages of spermatogenesis and the morphology of spermatozoa were normal (***Fig. 7E***). Additionally, CASA results confirmed that no statistical changes occurred in the concentration and percentage of motile spermatozoa from *Tmsb15a*$^{-/Y}$ mice compared with control mice (***Fig. 7F*** and ***7G***).

Discussion

Male infertility is a complex condition influenced by multiple factors, with genetic disorders identified as one of the primary contributors[2]. Our genome-wide association studies (GWAS) have identified numerous common variants associated with male infertility[25–28]. Additionally, rare variants in multiple genes have also

been reported whose impairment in function may result in male infertility[29–32]. Nevertheless, the pathogenic mechanisms underlying the condition in many affected individuals remain poorly understood[33]. Therefore, screening the function of genes that play essential roles in male reproduction using mouse models can significantly enhance our understanding of the etiology of male infertility[34–35]. In the current study, we generated six mutated mouse lines using the CRISPR/Cas9 system and demonstrated that these genes are not individually essential for male reproduction, suggesting that these genes may also not play critical roles in male fertility.

Among the six mutant mouse lines, we observed that *Tekt3* knockout significantly reduced sperm motility, although mutant males remained fertile. This phenomenon may be attributed to several compensatory mechanisms. First, maintenance of sperm count and mating behavior may compensate for the impaired motility. Despite reduced sperm motility, normal sperm counts likely ensure a sufficient number of gametes to sustain fertility. A previous study reported that double knockout of *Tekt3* and *Tekt4* led to reduced average litter size without altering total monthly offspring[36], suggesting that mating behavior may play a compensatory role. Second, functional redundancy among Tektin family members may contribute. Cao *et al*[37] demonstrated that *Tekt3* co-localizes with *Tekt1*, *Tekt2*, *Tekt4*, and *Tekt5* in the peri-axonemal accessory structures of the flagellum. Therefore, we hypothesize that other Tektins may partially compensate for Tekt3 deficiency, preserving normal fertility in mice.

The current study primarily investigates the phenotypic effects of individual knockouts of six genes, without exploring potential synergistic interactions. Given possible redundant or cooperative functions, combined knockouts may reveal abnormal reproductive phenotypes. Future studies could also explore synergistic regulatory mechanisms among these genes to further elucidate the molecular basis of spermatogenesis and male fertility.

Several traditional strategies have been used to identify candidate pathogenic genes associated with male infertility. These include: (1) conducting whole-exome or whole-genome sequencing in patients to detect pathogenic variants, followed by prioritizing candidate genes based on conservation scores and expression patterns, with subsequent functional validation in mouse models[38]; and (2) investigating genes with unknown functions or of particular interest within known biological pathways related to spermatogenesis, such as piRNA pathways and RNA-binding proteins[39–40], followed by reproductive phenotype analysis in mouse models. However, candidate pathogenic genes identified by these approaches often do not consistently impact male fertility in mouse models as anticipated. New strategies are needed.

We propose that supervised machine learning could be applied to identify essential genes for male reproduction. A study used an ensemble machine learning approach to predict meiosis-essential proteins based on their distinct abundance patterns, improving identification from 6.54% to 49.30%, with four of 10 mutant mice showing meiotic arrest in validation[41]. Although the identification rate still could not reach 100%, finding a new approach to more accurately predict the function of a given gene could substantially enhance our understanding of the functions of previously uncharacterized genes.

Human-mouse heterogeneity presents an unavoidable challenge in studying pathogenic genes associated with male infertility, contributing significantly to the discrepancy where genes identified as risk factors in humans often fail to exhibit abnormal reproductive phenotypes in mouse models. Despite approximately 99% sequence homology between humans and mice[9], the genetic basis of human male infertility is highly heterogeneous, involving complex multigenic interactions and environmental factors[42]. In contrast, mouse models often rely on single-allele knockouts or mutations, which may fail to fully recapitulate this complexity. For example, we did not detect abnormal reproductive phenotypes in these six mutant mouse models, while non-obstructive azoospermia patients do carry pathogenic loss-of-function variants in these genes (***Supplementary Table 6***). Another potential explanation is the unique epigenetic regulation and transcriptional dynamics involved in human spermatogenesis, which may not be fully replicated by the expression patterns or functions of specific key genes in mice[43]. Perhaps integrating human and mouse transcriptomic and proteomic data into the training of machine learning models could help bridge the gap caused by the heterogeneity between humans and mice, thereby enhancing the translatability of findings from mouse models to humans.

In summary, we identify six genes that are not essential for male fertility in mice. The current study focused solely on reproductive phenotypes, without detecting abnormalities in other systems. Therefore, all lines will be made available as bioresources for further analysis by other researchers. Publishing these results on non-essential genes can help other research

communities save time and avoid redundant effort. Consequently, if variants are identified in these six genes by whole-exome sequencing or whole-genome sequencing, these six genes may be deprioritized, and emphasis should be placed on other potentially causative genes and variants.

Fundings

This work was funded by grants from the National Natural Science Foundation of China (Grant No. 82495190 to Y.G.).

Acknowledgments

We are grateful to all colleagues and staff who contributed to this study.

Author contributions

Heling Fu: Investigation, Validation, Writing—original draft. **Haoran Chen**: Investigation, Writing—original draft. **Chenmeijie Li**: Investigation, Writing —original draft. **Shuai Lu**: Investigation, Writing —review & editing. **Yayun Gu**: Writing —review & editing. **Zhibin Hu**: Conceptualization, Supervision, Project administration.

Additional information

The online version contains supplementary material available at http://www.jbr-pub.org.cn/article/doi/10.7555/JBR.39.20250247. The data and materials used in this article will be shared on reasonable request to the lead contact, Zhibin Hu (zhibin_hu@njmu.edu.cn).

References

[1] Agarwal A, Baskaran S, Parekh N, et al. Male infertility[J]. *Lancet*, 2021, 397(10271): 319–333.

[2] Houston BJ, Riera-Escamilla A, Wyrwoll MJ, et al. A systematic review of the validated monogenic causes of human male infertility: 2020 update and a discussion of emerging gene-disease relationships[J]. *Hum Reprod Update*, 2021, 28(1): 15–29.

[3] Li C, Shen C, Xiong W, et al. *Spem*2, a novel testis-enriched gene, is required for spermiogenesis and fertilization in mice[J]. *Cell Mol Life Sci*, 2024, 81(1): 108.

[4] Huang Q, Liu Y, Zhang S, et al. Autophagy core protein ATG5 is required for elongating spermatid development, sperm individualization and normal fertility in male mice[J]. *Autophagy*, 2021, 17(7): 1753–1767.

[5] Ma A, Yang Y, Cao L, et al. FBXO47 regulates centromere pairing as key component of centromeric SCF E3 ligase in mouse spermatocytes[J]. *Commun Biol*, 2024, 7(1): 1099.

[6] Lu S, Gu Y, Wu Y, et al. Bi-allelic variants in human *WDR63* cause male infertility *via* abnormal inner dynein arms assembly[J]. *Cell Discov*, 2021, 7(1): 110.

[7] Qin D, Gu Y, Zhang Y, et al. Phase-separated CCER1 coordinates the histone-to-protamine transition and male fertility[J]. *Nat Commun*, 2023, 14(1): 8209.

[8] Houston BJ, Conrad DF, O'Bryan MK. A framework for high-resolution phenotyping of candidate male infertility mutants: From human to mouse[J]. *Hum Genet*, 2021, 140(1): 155–182.

[9] Lu Y, Oura S, Matsumura T, et al. CRISPR/Cas9-mediated genome editing reveals 30 testis-enriched genes dispensable for male fertility in mice[J]. *Biol Reprod*, 2019, 101(2): 501–511.

[10] Sun J, Lu Y, Nozawa K, et al. CRISPR/Cas9-based genome editing in mice uncovers 13 testis- or epididymis-enriched genes individually dispensable for male reproduction[J]. *Biol Reprod*, 2020, 103(2): 183–194.

[11] Oyama Y, Miyata H, Shimada K, et al. CRISPR/Cas9-mediated genome editing reveals 12 testis-enriched genes dispensable for male fertility in mice[J]. *Asian J Androl*, 2022, 24(3): 266–272.

[12] Heshmatnia F, Jafari M, Bozorgian L, et al. Is there a relationship between assisted reproductive technology and maternal outcomes? A systematic review of cohort studies[J]. *Int J Reprod Biomed*, 2023, 21(11): 861–880.

[13] Marleen S, Kodithuwakku W, Nandasena R, et al. Maternal and perinatal outcomes in twin pregnancies following assisted reproduction: A systematic review and meta-analysis involving 802 462 pregnancies[J]. *Hum Reprod Update*, 2024, 30(3): 309–322.

[14] Pandey S, Shetty A, Hamilton M, et al. Obstetric and perinatal outcomes in singleton pregnancies resulting from IVF/ICSI: A systematic review and meta-analysis[J]. *Hum Reprod Update*, 2012, 18(5): 485–503.

[15] Ahmad S, Jose da Costa Gonzales L, Bowler-Barnett EH, et al. The UniProt website API: Facilitating programmatic access to protein knowledge[J]. *Nucleic Acids Res*, 2025, 53(W1): W547–W553.

[16] Pusapati GV, Hughes CE, Dorn KV, et al. EFCAB7 and IQCE regulate hedgehog signaling by tethering the EVC-EVC2 complex to the base of primary cilia[J]. *Dev Cell*, 2014, 28(5): 483–496.

[17] Liu Y, Li Y, Meng L, et al. Bi-allelic human *TEKT3* mutations cause male infertility with oligoasthenoteratozoospermia owing to acrosomal hypoplasia and reduced progressive motility[J]. *Hum Mol Genet*, 2023, 32(10): 1730–1740.

[18] Stauber M, Weidemann M, Dittrich-Breiholz O, et al. Identification of FOXJ1 effectors during ciliogenesis in the

foetal respiratory epithelium and embryonic left-right organiser of the mouse[J]. *Dev Biol*, 2017, 423(2): 170–188.

[19] Yamashita T, Liu J, Gao J, et al. Essential and synergistic roles of RP1 and RP1L1 in rod photoreceptor axoneme and retinitis pigmentosa[J]. *J Neurosci*, 2009, 29(31): 9748–9760.

[20] Rodríguez de la Vega Otazo M, Lorenzo J, Tort O, et al. Functional segregation and emerging role of cilia-related cytosolic carboxypeptidases (CCPs)[J]. *FASEB J*, 2013, 27(2): 424–431.

[21] Wang C, Gu Y, Zhang K, et al. Systematic identification of genes with a cancer-testis expression pattern in 19 cancer types[J]. *Nat Commun*, 2016, 7: 10499.

[22] Kunimoto K, Yamazaki Y, Nishida T, et al. Coordinated ciliary beating requires *Odf2*-mediated polarization of basal bodies *via* basal feet[J]. *Cell*, 2012, 148(1-2): 189–200.

[23] Sheridan J, Grata A, Dorr J, et al. Centriolar defects underlie a primary ciliary dyskinesia phenotype in an adenylate kinase 7 deficient ciliated epithelium[J]. *Dev Biol*, 2025, 524: 152–161.

[24] Yang X, Wang Q, Li T, et al. A splicing variant in *EFCAB7* hinders ciliary transport and disrupts cardiac development[J]. *J Biol Chem*, 2025, 301(3): 108249.

[25] Jiang T, Wang Y, Zhu M, et al. Transcriptome-wide association study revealed two novel genes associated with nonobstructive azoospermia in a Chinese population[J]. *Fertil Steril*, 2017, 108(6): 1056–1062.e4.

[26] Ni B, Lin Y, Sun L, et al. Low-frequency germline variants across 6p22.2–6p21.33 are associated with non-obstructive azoospermia in Han Chinese men[J]. *Hum Mol Genet*, 2015, 24(19): 5628–5636.

[27] Hu Z, Li Z, Yu J, et al. Association analysis identifies new risk loci for non-obstructive azoospermia in Chinese men[J]. *Nat Commun*, 2014, 5: 3857.

[28] Hu Z, Xia Y, Guo X, et al. A genome-wide association study in Chinese men identifies three risk loci for non-obstructive azoospermia[J]. *Nat Genet*, 2011, 44(2): 183–186.

[29] Kherraf ZE, Cazin C, Bouker A, et al. Whole-exome sequencing improves the diagnosis and care of men with non-obstructive azoospermia[J]. *Am J Hum Genet*, 2022, 109(3): 508–517.

[30] Lillepea K, Juchnewitsch AG, Kasak L, et al. Toward clinical exomes in diagnostics and management of male infertility[J]. *Am J Hum Genet*, 2024, 111(5): 877–895.

[31] Nagirnaja L, Lopes AM, Charng WL, et al. Diverse monogenic subforms of human spermatogenic failure[J]. *Nat Commun*, 2022, 13(1): 7953.

[32] Gao Y, Liu L, Shen Q, et al. Loss of function mutation in *DNAH7* induces male infertility associated with abnormalities of the sperm flagella and mitochondria in human[J]. *Clin Genet*, 2022, 102(2): 130–135.

[33] Oud MS, Ramos L, O'Bryan MK, et al. Validation and application of a novel integrated genetic screening method to a cohort of 1 112 men with idiopathic azoospermia or severe oligozoospermia[J]. *Hum Mutat*, 2017, 38(11): 1592–1605.

[34] Matzuk MM, Lamb DJ. The biology of infertility: Research advances and clinical challenges[J]. *Nat Med*, 2008, 14(11): 1197–1213.

[35] Kent K, Johnston M, Strump N, et al. Toward development of the male pill: A decade of potential non-hormonal contraceptive targets[J]. *Front Cell Dev Biol*, 2020, 8: 61.

[36] Roy A, Lin YN, Agno JE, et al. Tektin 3 is required for progressive sperm motility in mice[J]. *Mol Reprod Dev*, 2009, 76(5): 453–459.

[37] Cao W, Gerton GL, Moss SB. Proteomic profiling of accessory structures from the mouse sperm flagellum[J]. *Mol Cell Proteomics*, 2006, 5(5): 801–810.

[38] Jiao S, Yang Y, Chen S. Molecular genetics of infertility: Loss-of-function mutations in humans and corresponding knockout/mutated mice[J]. *Hum Reprod Update*, 2021, 27(1): 154–189.

[39] Stallmeyer B, Bühlmann C, Stakaitis R, et al. Inherited defects of piRNA biogenesis cause transposon de-repression, impaired spermatogenesis, and human male infertility[J]. *Nat Commun*, 2024, 15(1): 6637.

[40] Li Y, Wang Y, Tan Y, et al. The landscape of RNA binding proteins in mammalian spermatogenesis[J]. *Science*, 2024, 386(6720): eadj8172.

[41] Fang K, Li Q, Wei Y, et al. Prediction and validation of mouse meiosis-essential genes based on spermatogenesis proteome dynamics[J]. *Mol Cell Proteomics*, 2021, 20: 100014.

[42] Guo J, Grow EJ, Mlcochova H, et al. The adult human testis transcriptional cell atlas[J]. *Cell Res*, 2018, 28(12): 1141–1157.

[43] Ha D, Kim D, Kim I, et al. Evolutionary rewiring of regulatory networks contributes to phenotypic differences between human and mouse orthologous genes[J]. *Nucleic Acids Res*, 2022, 50(4): 1849–1863.

[44] Cardoso-Moreira M, Halbert J, Valloton D, et al. Gene expression across mammalian organ development[J]. *Nature*, 2019, 571(7766): 505–509.